scientific reports

Check for updates

OPEN

Role of organic cation orientation in formamidine based perovskite materials

Siyu Liu[1], Jing Wang[2], Zhe Hu[2], Zhongtao Duan[1], Hao Zhang[3], Wanlu Zhang[2], Ruiqian Guo[1,2]✉ & Fengxian Xie[1,2]✉

The rotation of organic cations is considered to be an important reason for the dynamic changes in stability and photoelectric properties of organic perovskites. However, the specific effect of organic cations rotation on formamidine based perovskite is still unknown. In our work, first-principles calculations based on density functional theory are used to examine the effect of the rotation of formamidine cations in $FAPbI_3$ and $FA_{0.875}Cs_{0.125}PbI_3$. We have comprehensively calculated the structure, electronic and optical properties of them. We found a coupling effect between formamidine cations rotation and cesium atom. This coupling effect changes the inclination angle of octahedron to regulate electron distribution, band gaps, and optical absorption. Hence, changing the cation orientation and substitution atom is a feasible way to dynamically adjust the energy band, dielectric constant and absorption edge of perovskite. Preparing perovskite with tunable properties is just around the corner through this way.

Since the concept of organic halide perovskite was proposed in 2013[1], it has drawn substantial interests for researchers from materials, chemistry and physics field[2]. In 2015, Nam-Gyu Park et al.[3] used 10% cesium to substitute formamidine cation and got lower trap-density, higher open circuit voltage, respectful thermal property and enhanced stability. Recently, as the efficiency of formamidine based perovskite materials has reached more than 20% efficiency and 3000 min T_{80} lifetime (the time that the solar cell can run at 80% of its initial performance)[4,5], they have been considered as promising candidates for new era perovskite materials.

Though researchers try hard to promote efficiency and improve stability of formamidine based perovskite materials, the mechanism for improving the efficiency and stability of perovskite materials and devices is still not clear. For instance, how the photoelectric properties and charge dynamics in perovskites be affected by specific mechanisms including the size, the interaction of organic cations and the interaction with the crystal structure. Some former study thought that the main function of organic cations is to stabilize the structure and will not change photoelectronic properties[6]. Mehdizadeh et al.[7] studied that the rotation of the MA in R_z and R_x modes causes substantial changes in the band structure, density of states, electron density, dielectric function, and absorption spectrum. They found that these changes are greatly affected by the interaction of cation–cation (MA-Pb) and cation–anion (MA-X) and van der Waals radius of organic cations. Researchers had also done related studies on the FA system and compared the differences from the MA system due to ion size, charge distribution and hydrogen bonding. Besides, the inorganic PbI_6 octahedral frame experienced Glazer tilt with a time of 0.2–1.5 ps in $MAPbI_3$, and the FA cation at A-site in $FAPbI_3$ rotates or rolls in the cage (2 – 3 ps), which indicates organic cations' orientation plays an important role in halide perovskite[8]. To be more specific, the orientation of organic cation has relations with ferroelectricity[9], ion transport[10], phase transition temperature[11], water molecule adsorption and device stability[12].

Recently, some researchers paid attention to this and used density functional theory (DFT) to describe this phenomenon in detail. Carlo et al.[13] revealed the role of organic cations in hybrid halide perovskite $MAPbI_3$. Furthermore, Jonathon et al.[14] considered the influence of the rotation of the MA cation along the coordinate axis and the coaxial precession on the performance of perovskite. Besides, Nathaniel et al.[15] considered the coupling effect between cations and inorganic lattice, the different energy barrier between FA and MA cation rotation. Akhtarianfar et al.[16] investigated the formamidine cation rotation in $FAPbI_3$. But there is no one has studied the effect of cation orientation on inorganic ions, perovskite lattice and properties in the FA/Cs system

[1]Institute of Future Lighting, Academy for Engineering and Technology, Fudan University, Shanghai 200433, China. [2]Institute for Electric Light Sources, School of Information Science and Technology, Fudan University, Shanghai 200433, China. [3]Department of Optical Science and Engineering, Fudan University, Shanghai 200433, China. ✉email: rqguo@fudan.edu.cn; xiefengxian@fudan.edu.cn

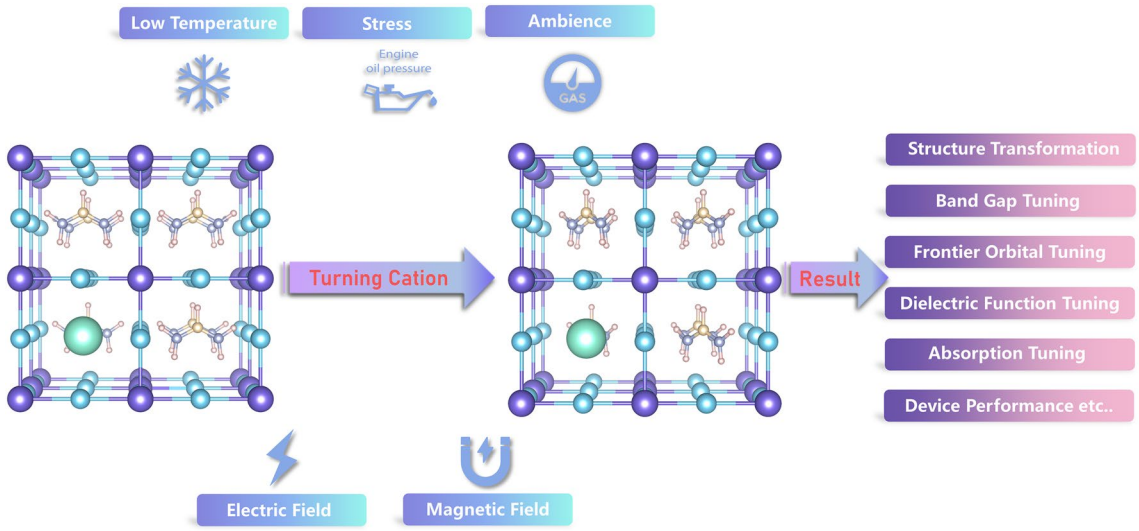

Figure 1. Schematic diagram of possible ways to change the orientation of organic cation and the result lead by it.

of formamidine based perovskite. On the other hand, studies show that the rotation of cations decreases at low temperature and high pressure[17,18], so it is possible to control the synthesis of cation-oriented cubic perovskite to bring vital different changes in this field.

Hence, our work is the first time to investigate the complex coupling effect of organic orientation in formamidine based perovskite. We used DFT theory to build a supercell to study this problem, and tried to build a reasonable explanation of it. We found that the coupling effect of organic cations and cesium atom affected many properties of this mixing system, such as lattice constant, band structures, charge distribution, dielectric constant, optical absorption properties, and even the performance of solar cell device (Fig. 1). Our work not only expounds the mechanism of the role of cation orientation in the mixed system, but also points out a feasible way for the synthesis of electron and optically adjustable perovskite materials and devices.

Computational details

All of these first-principles calculations were performed by using the Vienna Ab initio Simulation Package (VASP)[19,20]. Perdew–Burke–Ernzerhof (PBE) exchange correlation functional was used within a generalized gradient approximation (GGA)[21] and optB86b[22] van der Waals force revision. We focused on the pseudo-cubic phase of formamidine based perovskite with the chemical structures of $FAPbI_3$ and $FA_{0.875}Cs_{0.125}PbI_3$. A cut-off energy of 400 eV was chosen to reach the desired accuracy. For the optimization of the geometric structure, the total energy convergence criterion was chosen as 10^{-5} eV, and the force on each atom was converged to an accuracy of 0.01 eV·Å^{-1}. The size of the $FAPbI_3$ supercell is $2\times2\times2$, and one formamidine is substituted by a cesium atom to simulate the 12.5% doping. A reciprocal-space sampling with gamma center in an $8\times8\times8$ Monkhorst–Pack k-point mesh[23] was set in the Brillouin zone for the standard DFT calculations. The occupied and empty bands set in the DFT calculation are 240 for $FAPbI_3$ and 224 for $FA_{0.875}Cs_{0.125}PbI_3$. Molecular dynamics simulation used canonical ensemble (NVT). The temperature of simulation is 400 K. The total simulation time of each trajectory was 5 ps with a 2 fs timestep. Considering the computational accuracy and the enormous demands of calculation resources, the phase of perovskite will change from high to low temperature, and VASP calculations are performed at 0 K, we did not calculate phonon spectrum and elastic constants. And to mitigate the effect due to the 0 K calculation, we used the crystal constant from experiment as the basis to build our model. The VESTA software was used to visualize crystal structures and electron distribution[24]. The VASPKIT toolkit was used to post-process the band gap, density of state and dielectric constant data[25].

For calculating cohesive energy E_c, the formula is as follows:

$$E_c = \frac{E\left(A_mB_nC_pD_q\right) - mE(A) - nE(B) - pE(C) - qE(D)}{\textit{The number of atoms in a conventional unit cell}} \tag{1}$$

where $E(A_mB_nC_pD_q)$ means the relaxed energy of structure, A, B, C, D are the elements in structure, m, n, p, q are the numbers of each element. $E(A), E(B), E(C), E(D)$ are the energy of single atom of each element.

For evaluating the optical properties, we calculated the frequency-dependent complex dielectric function[26].

$$\varepsilon(\omega) = 1 + \frac{8\pi}{\Omega N_k}\sum_{k,v,c}\frac{\left|\langle\varphi_{kv}\left|\widehat{v}\right|\varphi_{kc}\rangle\right|^2}{(E_{kc}-E_{kv})^2(E_{kc}-E_{kv}-\omega-i\eta)} \tag{2}$$

System	Orientation	Lattice constant (Å)	Cell volume (Å^3)	Distortion index (bond length)	Relaxed energy (eV)	Cohesive energy (eV)
$FAPbI_3$	(100)	12.6211	2010.4645	0.00935	− 340.5251	− 3.4751
	(110)	12.4713	1939.6834	0.00701	− 340.8722	− 3.4787
	(111)	12.5371	1970.5563	0.01219	− 340.6713	− 3.4767
$FA_{0.875}Cs_{0.125}PbI_3$	(100)	12.6140	2007.0482	0.01096	− 301.7401	− 3.3029
	(110)	12.4839	1945.5874	0.00764	− 301.9107	− 3.3048
	(111)	12.5377	1970.8478	0.00938	− 301.7699	− 3.3032

Table 1. Calculated lattice constant, cell volume, distortion index (bond length) and relaxed energy of $FAPbI_3$ and $FA_{0.875}Cs_{0.125}PbI_3$.

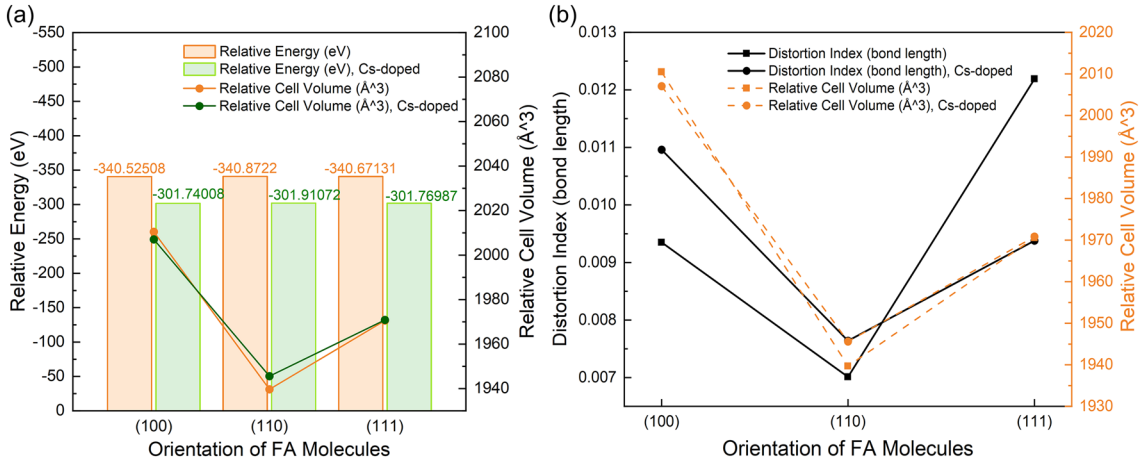

Figure 2. (**a**) Relative energy and relative cell volume in different FA cations orientation; (**b**) relative energy and distortion index (bond length) in different FA cations orientation.

where Ω is the volume of the cell, $\hat{v}$ is the operator of velocity,η is an opportune broadening factor, N_k is the total number of k-points in the Brillouin zone, and the indices c and v show the unoccupied and occupied states, respectively. The frequency-dependent absorption coefficient $\alpha(\omega)$, is given by

$$\alpha(\omega) = \omega\sqrt{\frac{-\mathrm{Re}\varepsilon(\omega) + \sqrt{\mathrm{Re}^2\varepsilon(\omega)} + \mathrm{Im}^2\varepsilon(\omega)}{2}}. \quad (3)$$

Results and discussion

Structural stability and adjustment. Figure S1 shows the initial 2×2×2 supercell of $FAPbI_3$ and $FA_{0.875}Cs_{0.125}PbI_3$ with formamidine cations facing the (100), (110) and (111) direction. Before all others, all the calculations have converged on the energy convergence standard 10^{-5} eV and the force convergence standard 0.01 eV·Å^{-1} per atom by using GGA-PBE exchange correlation functional[21] with van der Waals force correlation[22] without considering the spin–orbit coupling (SOC). We also calculated cohesive energy and ab-initio molecular dynamics (AIMD) in 400 K to confirm the dynamical stability of these hybrid perovskites[27,28]. The cohesive energy of all our structures is less than zero, which means these structures are stable in 0 K. The energy-time curves of AIMD of all our structures are straight, which means these structures are stable in 400 K (Table 1; Figure S2).

In Table 1 and Fig. 2, the data of relaxed structures for the cubic phase of $FAPbI_3$ and $FA_{0.875}Cs_{0.125}PbI_3$ are displayed. Refer to previous research, PBE-vDW method can obtain the most accurate lattice constant than DFT-PBE and HSE06 methods in formamidine halide perovskite[29]. The lattice constant of $FAPbI_3$ supercell we calculated in (100) direction is close to antecedent experiment[30,31] and calculation[29]. We used the cell volume and lattice constant obtained by the cube root of cell volume for measuring the disorder of the structure due to the structure will turn from cubic phase to pseudo-cubic phase[32]. Therefore, we have reason to believe that our model effectively represents the specific case of an actual condition of perfectly aligned molecular dipoles.

Firstly, let us separately discuss changes lead by orientation in $FAPbI_3$ and $FA_{0.875}Cs_{0.125}PbI_3$ system. From Fig. 2a, we can discover that the relaxed energy at each formamidine orientation is similar, and the energy barrier is 0.2–0.3 eV for each condition. It's not a tremendous energy barrier, so formamidine cations can freely rotate in cage. According to previous research, the formamidine cations are indeed rapid rotating with a time period of 2–3 ps and PbI_6 octahedral framework is undergoing Glazer tilting with a time period of about 0.2–1.5 ps[17,33].

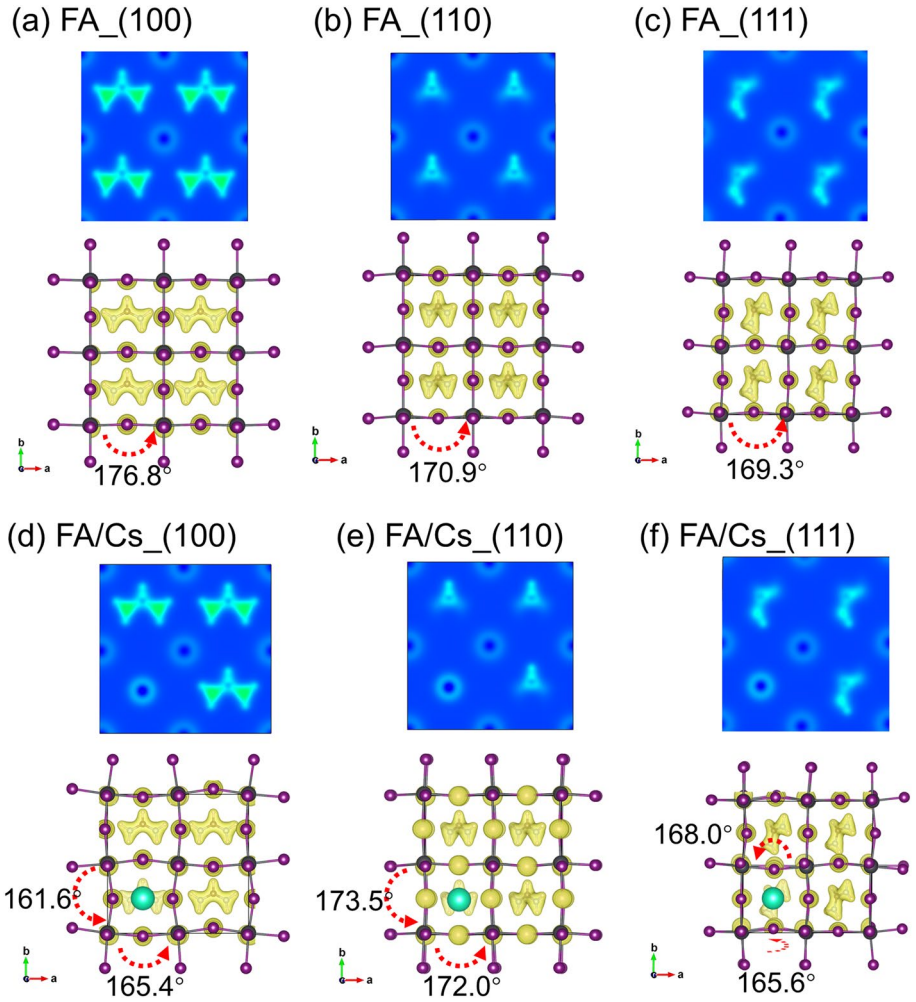

Figure 3. Two-dimensional (2D) depiction of electron charge density in crystallographic plane of (001) in $FAPbI_3$ (**a**) (100), (**b**) (110), (**c**) (111) and $FA_{0.875}Cs_{0.125}PbI_3$, (**d**) (100), (**e**) (110), (**f**) (111). 3D charge map is also shown for each sub-figure.

Besides the relaxed energy, the relative cell volume of (110) is the smallest in three rotation models, leading to the minimum of lattice constant. The change of lattice constant in $FAPbI_3$ system is affected by the reorientation of formamidine cations because their atom arrangement and charge distribution are anisotropic. These factors cause Pb–I–Pb to be subject to different forces like N–H···I hydrogen bond and van der Waals force in different directions[34]. Furthermore, the contraction of perovskite lattice from $FAPbI_3$ to $FA_{0.875}Cs_{0.125}PbI_3$ is usually attributed to the substitution from formamidine to cesium because of the smaller radius of cesium[35]. In fact we indeed find that the lattice constant of $FA_{0.875}Cs_{0.125}PbI_3$ in (100) direction has a 0.1% decrease than $FAPbI_3$, which is consistent with the experiment[36]. But the phenomenon in (110) and (111) is different. This difference can be attributed to the coupling effect between the orientation of organic cations and the addition of cesium.

This coupling effect also influences the tilt of PbI_6 octahedron. From Fig. 2b, both $FAPbI_3$ and $FA_{0.875}Cs_{0.125}PbI_3$ systems get the minimum value of distortion index (this index describes the degree of tilt of PbI_6 octahedron) in (110) direction. We can also directly see the degree of deformation in Figure S3. The difference is that $FAPbI_3$ gets the maximum value in (111) direction but $FA_{0.875}Cs_{0.125}PbI_3$ gets it in (100) direction, which maybe lead by the cesium and formamidine cations co-effect.

All in all, the reorientation of formamidine cations and the entrance of cesium give the formamidine perovskite adjustment structural properties. Lots of researches before shows that organic cations will be 'frozen' in low temperature[14,37,38]. And the structural stability is also be closely bound up with the internal structure of perovskite. Therefore, our work indicate which low temperature state is good for the application in different areas.

Electronic properties. Figure 3 shows the 2D and 3D maps of electron charge density. This map reveals the interaction among the components of the perovskite and how electrons distribute in the lattice. We set the isosurface level 0.1 electrons/bohr^3 to see the distribution more directly.

According to the non-doped $FAPbI_3$ perovskite, the interaction of formamidine with PbI_6 octahedron leads to a considerable disorder, which alters its volume (cell volume is changed as well) (refer to Table 1; Fig. 2). Interestingly, Table 1 tells us the distortion of PbI_6 octahedron reaches a minimum in (110) direction. This phenomenon

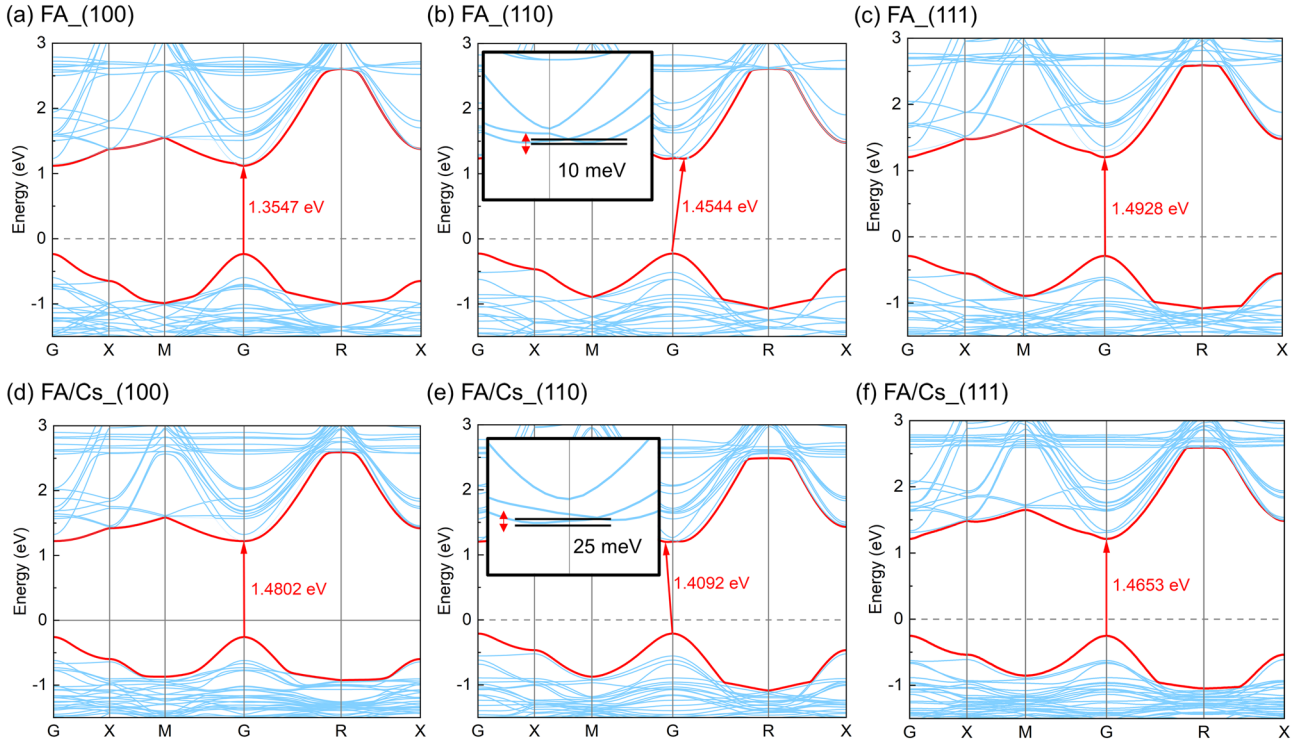

Figure 4. (**a**–**c**) Band gap of $FAPbI_3$ with different FA cations orientation: (**a**) (100), (**b**) (110), (**c**) (111); (**d**–**f**) band gap of $FA_{0.875}Cs_{0.125}PbI_3$ with different FA cations orientation: (**d**) (100), (**e**) (110), (**f**) (111).

can be attributed to that the symmetrical interactions in (110) plane uniformly inflate the size of PbI_6, which leads to a decrease of PbI_6 distortion degree compared with other orientations[7].

Moreover, the $FA_{0.875}Cs_{0.125}PbI_3$ system shows some similarities and differences. Diverse directions indeed tilt the PbI_6 octahedron and Pb–I–Pb bond angle, but the addition of cesium also affects them. It's obviously that the cesium atom shows strong ionization because the light around the cesium atom is weak in 2D contour plot Fig. 3d–f. This is because the electronegativity of cesium is near the largest in periodic table, and the electron in Cs 6s orbit is easy to be seized and lose. Owing to this, the bond angle of Pb–I–Pb is strongly tilted when formamidine cations orient to (100) direction. In (110) direction, the distortion reduces than (100) orientation, and we can see the bond angle of Pb–I–Pb is tilting slightly than (100) orientation. This reduction maybe is the same reason like $FAPbI_3$ we discussed below. But the $FA_{0.875}Cs_{0.125}PbI_3$ system's distortion index is larger than $FAPbI_3$ system when orients to (110) direction, which is caused by the smaller radius of cesium. When turns to (111) direction, the Pb–I–Pb bond occurs inner fold on x–y plane with a 7.8° angle but the distortion is smaller than $FAPbI_3$ in the same direction. This is because the substitution of cesium reduces the charge interaction lead by (111) direction of formamidine cations. To be more specific, the (111) orientation of formamidine causes a catercorner electronic interaction, but cesium atom also possesses a strong polarization force. The coupled effect of them leads to this result, and even affects the bandgap and density of state we will discuss after.

Now let's focus on the role of formamidine orientation in electronic structure. Figures 4, 5 and 6 shows the band structure and density of state (DOS) of formamidine based perovskite. Figure 4 indicates the trends of band gap of $FAPbI_3$ and $FA_{0.875}Cs_{0.125}PbI_3$. Since spin–orbit coupling (SOC) will change the band gap, and GGA will underestimate the band gap, the effects of them coincidentally make the band gap calculated without considering the SOC close to the experimental value[32,34,39]. While using HSE06 + SOC can get a more accurate value, we just want to focus on the variation of band gap. Hence, it's enough for us to use the result of PBE-vDW function.

From Fig. 4, we can see that the band gap of $FAPbI_3$ increases from (100) to (110) and to (111) direction, while the band gap of $FA_{0.875}Cs_{0.125}PbI_3$ decreases first and then increases. In both models, the band gap in the (110) direction changes from direct to indirect. We propose that the reasons for these phenomena may be as follows: (1) the distortion of PbI_6 octahedron; (2) the addition of cesium atom; (3) the dispersive force between the organic cations and the inorganic framework.

First and foremost, the lattice contraction is affected by the A-site cation radius. If the perovskite lattice contracts, the band gap will increase. That's why the band gap of $FA_{0.875}Cs_{0.125}PbI_3$ will increase from 1.3547 eV of $FAPbI_3$ to 1.4802 eV in (100) direction. Moreover, metal-halide orbital overlap is a σ^* interaction, decreasing the Pb–I–Pb bond angle will reduce the degree of overlap between the metal and halide orbitals[40]. The result is that when cesium substitution increases, the valence band moves to a slightly lower energy (see in Fig. 5; Table S1), thereby widening the band gap. This phenomenon is consistent with the Cs-doped experiment[3,35,36].

Secondly, the tilt of the PbI_6 octahedron can change the spatial distribution and overlap of electron orbits, and this tilting effect depends on the electronic interaction between ions. This condition is well known as the dipole coupling effect lead by the number of ^1H-^1H dipolar couplings on adjacent cations[41]. From Table S1 and

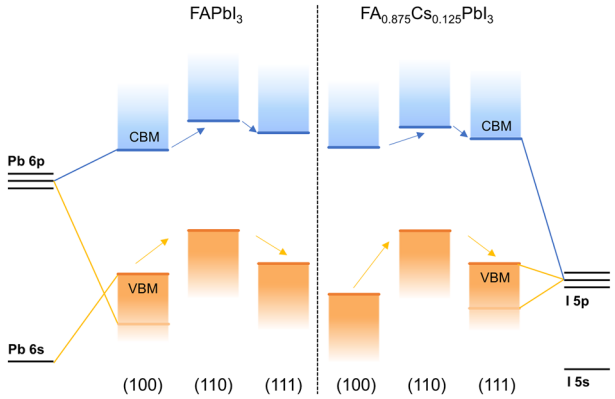

Figure 5. Schematic energy level diagram of different formamidine orientations (black line: atom energy level; blue line: valence band minimum; orange line: conduction band maximum; black dotted line: fermi energy).

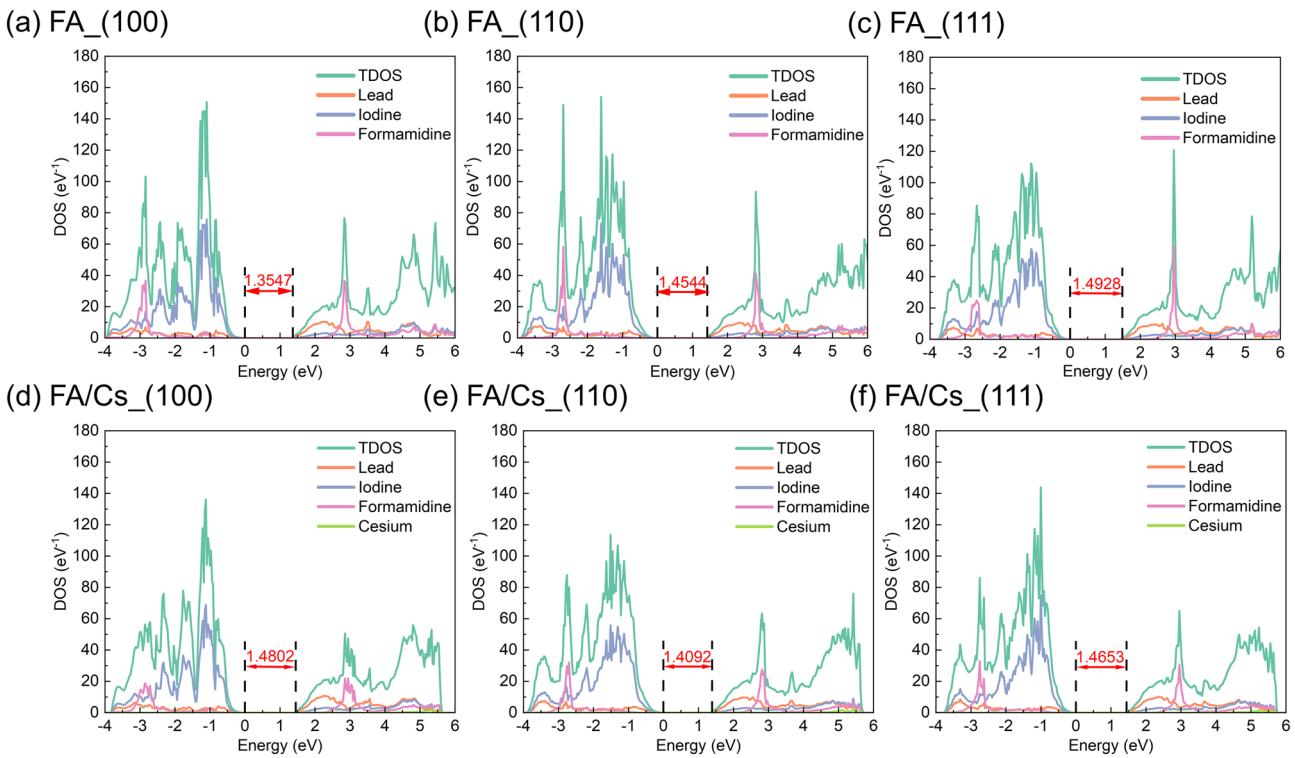

Figure 6. Total density of state (TDOS) and projected density of state (PDOS): (**a**–**c**) $FAPbI_3$ with different FA cations orientation: (**a**) (100), (**b**) (110), (**c**) (111); (**d**–**f**) $FA_{0.875}Cs_{0.125}PbI_3$ with different FA cations orientation: (**d**) (100), (**e**) (110), (**f**) (111).

Fig. 4b,c, the band gap increases though the lattice constant contract, which can be attributed to the turning of formamidine cations from (110) to (111) direction enhances the dipole–dipole interaction and the distortion index. Meanwhile, from Table 1 and Fig. 4d–f, the smaller size of cesium and the largest distortion index increase the band gap in (100) direction. But the reorientation decreases the distortion index, leading to the reduction of band gap in (110) and (111) directions. Besides, the addition of cesium decreases the number of N–H···I hydrogen bond[14,33], and this influence may enlarge in (110) and (111) directions. Hence, the band gap reduces and even is smaller than the $FAPbI_3$ system in these two directions.

Thirdly, the dispersive force between the organic cations and the inorganic framework leads to the gap transformation from direct to indirect in (110) direction of both systems (see in Fig. 4b,e). Carlo et al.[13] firstly discovered and demonstrated this change when viewing the turning of methylamine cations in $MAPbI_3$. Then Farshad et al.[16] also found this phenomenon in $FAPbI_3$. Besides, the static effects, such as Rashba splitting in the conduction band may play an effective role in VBM[42]. At our work, we also observed 10 meV and 25 meV

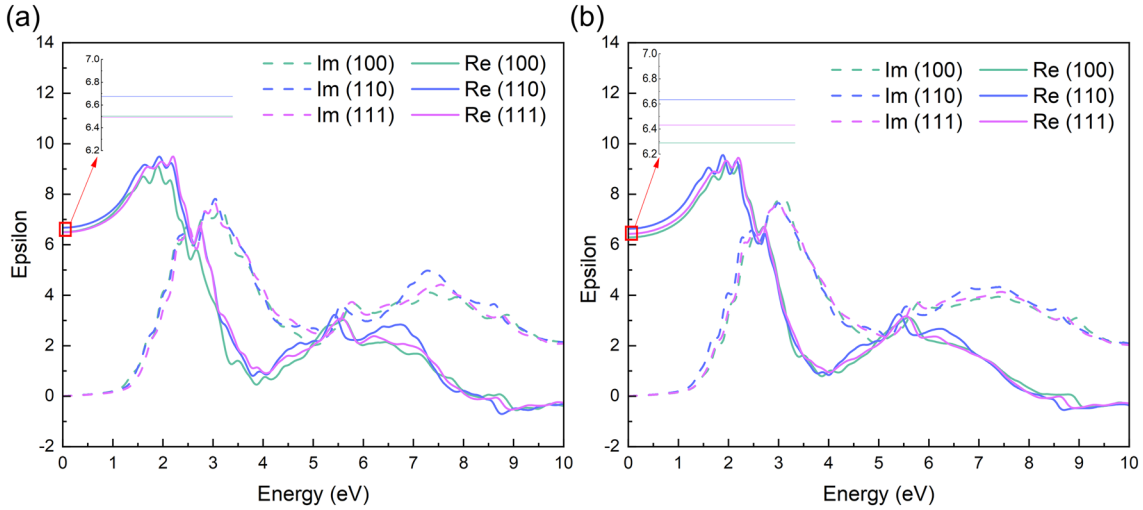

Figure 7. The real and imaginary part of dielectric function of (**a**) $FAPbI_3$ and (**b**) $FA_{0.875}Cs_{0.125}PbI_3$ with different FA cations orientation.

departure of VBM in (110) direction of $FAPbI_3$ and $FA_{0.875}Cs_{0.125}PbI_3$. This change may have a potential impact on the transport and recombination of carriers.

From Fig. 5, we can see that the orientation of formamidine cations not only affect the band gap, but also turn the VBM, CBM and Fermi energy. They are rising first and then falling in general and the trend is accordant in both systems. Recently, band gap engineering is popular[40,43,44]. Researchers achieved high efficiency by turning perovskite band gap alignment with ETL or HTL layer. If we can control the band gap by turning the intrinsic organic cation, it's a new idea to achieve higher carrier mobility, J_{sc}, V_{oc} and efficiency.

As is well-known that the CBM is mainly contributed by the electrons of the Pb 6p orbitals, and the VBM mainly is contributed by the electrons of I 5p orbitals. From the PDOS result in Fig. 6, we indeed find that the frontier orbitals are composed of Pb atom and I atom.

In addition, the difference between energy state below and above the Fermi energy means the bang gap, and it's consistent with the result of band gap in Fig. 4. Besides, comparing Fig. 6a–c and Fig. 6d–f, the addition of cesium atom makes the total DOS distribution more localized around the Fermi energy, which enhances ionic interaction though the electrons of cesium do not distribute in frontier orbitals (Fig. 6d–f). This is thought that the addition of cesium makes perovskite structure more stable[8]. Moreover, the turning of orientation from (100) to (111) in Fig. 6a–c makes the formamidine density of state in about 3 eV deep conduction band stronger. This condition is the same with Cs-doped system. This confirms the interaction between formamidine and PbI_6 framework. Compared with the same direction of $FAPbI_3$ and $FA_{0.875}Cs_{0.125}PbI_3$, cesium atom exists in deeper conduction bands, and the energy state distribution is deep than 5 eV. Cesium ion exhibits strong ionization and this may contribute to other atoms' charge distribution in space and the stability of the structure.

Optical properties. With the special electronic structure, $FAPbI_3$ also has fantastic ability of optical absorption in the visible range used in solar cell and light emitting diode. Many features of $FAPbI_3$, such as excellent stability under high humidity, sharper absorption edge, high charge mobility and low exciton binding energy can be attributed to the high dielectric constant of the material[45]. The coupling effect of organic cation orientation and the substitution of cesium can also be observed in optical properties. The reorientation of the organic cation and the addition of cesium with their correlated dipole moment dedicates to the dielectric response and throw a crystal field to formamidine based perovskite[7]. To study the role of organic cation with cesium atom, we calculated dielectric function in Fig. 7 and absorption spectrum in Fig. 8 for $FAPbI_3$ and $FA_{0.875}Cs_{0.125}PbI_3$ in (100), (110) and (111) direction.

Figure 7 shows the real and imaginary part of dielectric function. Generally speaking, the real part of dielectric function represents static dielectric constant at $E = 0$, which is calculated to be 6.50, 6.68 and 6.49 for $FAPbI_3$ and 6.29, 6.63 and 6.43 for $FA_{0.875}Cs_{0.125}PbI_3$ in (100), (110) and (111) direction (inset zoomed pictures of Fig. 7; Table S2). It's obviously that the rotation of formamidine cations change the static dielectric constant in different orientation, and the entrance of cesium contracts the value of static dielectric constant compared with $FAPbI_3$. This transformation definitely influences the optical properties like absorption in Fig. 8. The dashed curves in Fig. 7a,b display imaginary part of dielectric function. And it's well known that the first peak represents as the direct optical transition, which is also called optical gap[7]. It can be seen in Fig. 7a that the rotation of formamidine cations from (100) to (111) leads to a blue shift in $FAPbI_3$. But a red shift occurs when formamidine cations rotate from (100) to (111) in $FA_{0.875}Cs_{0.125}PbI_3$. This is as well as the trends of band gap and absorption spectrum.

From Fig. 8, the inset zoomed pictures show band edge absorption condition, which has a strong correlation with band gap. All of these same trends prove the orientation of formamidine cations and the addition of cesium exist coupling effect. Besides, the after peak sometimes is thought as the exciton emission peak in quantum dot perovskite[46].

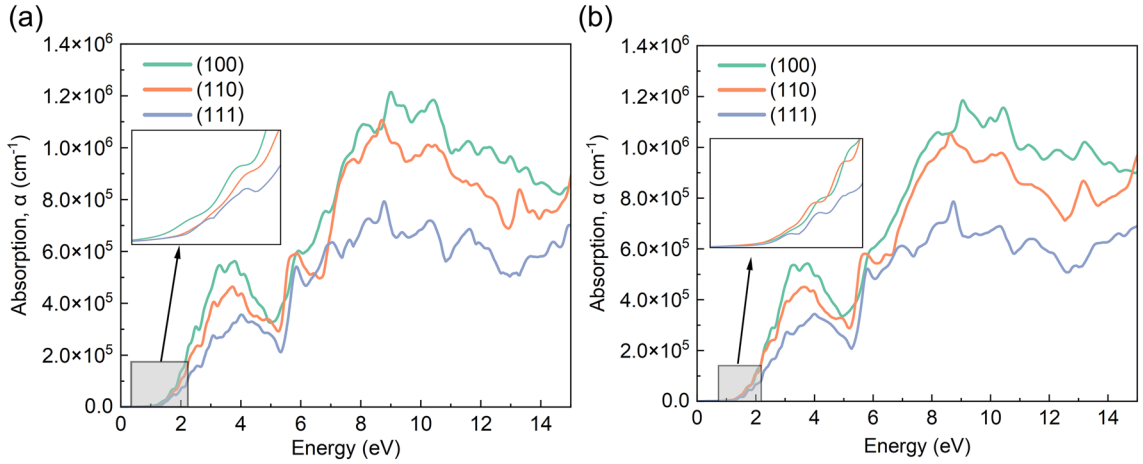

Figure 8. Optical adsorption spectrum of perovskite structures of (**a**) $FAPbI_3$ and (**b**) $FA_{0.875}Cs_{0.125}PbI_3$ with different FA cations orientation.

Hence, the coupling effect of organic cation orientation and the substitution of cesium makes the optical performance of the mixed cation halide perovskite tunable. This is a crucial and promising method for manufacturing light-absorbing devices with variable intrinsic properties.

Conclusions

Today, the efficiency and stability of formamidine based perovskite materials have been rapidly improved, but there are still many unsolved mysteries in the theories used to explain its advantages over other materials. Our work suggests that the size of PbI_6 octahedron, lattice constant, charge distribution, band gap, density of state and absorption spectrum are inseparable from the orientation of organic cations and its coupling with cesium atom.

To be more specific, when the cation rotates from (100) to (110) and then to (111), the lattice constant and distortion index of FA and FA/Cs systems both decrease first and then increase. Although the minimum point is the same, the distortion index of the (111) plane in the FA/Cs system is abnormally smaller than the FA system due to the interaction between FA orientation and Cs. These results are due to the orientation of cations and the addition of cesium atom, which change the forces between ions in the crystal lattice, such as van der Waals forces and N–H···I hydrogen bonds.

In regard to electronic and optical properties, the different orientations of FA lead to changes in the band gap. Particularly, in the (110) direction, the band gap of the formamidine based perovskite becomes indirect. The addition of Cs also changes the band gap. We summarize the reasons into the following three points: (1) the distortion of PbI_6 octahedron; (2) the addition of cesium atom; (3) the dispersive force between the organic cations and the inorganic framework. Moreover, the orientation of FA changes the distribution of electrons in the frontal orbit, while the addition of Cs makes it more localized and concentrated near the band gap. Furthermore, the orientation of FA changes the energy level of CBM, VBM and Fermi energy, which can provide a new idea for the experiment of band gap adjustment and alignment. Eventually, the orientation of FA and the doping of Cs also change the dielectric constant and the peak of the optical absorption spectrum.

Overall, this work starts from the formamidine rotation and its interaction with cesium atom. We demonstrate a possible way to engineer lattice constant, band gap, density of state and absorption spectrum, which is a prerequisite for controllable variable high-efficiency optoelectronic device.

Data availability

The datasets generated during and/or analyzed during the current study are available from the corresponding author on reasonable request.

Received: 27 June 2021; Accepted: 27 September 2021
Published online: 14 October 2021

References

1. Gao, P., Grätzel, M. & Nazeeruddin, M. K. Organohalide lead perovskites for photovoltaic applications. *Energy Environ. Sci.* **7**, 2448–2463. https://doi.org/10.1039/C4EE00942H (2014).
2. Dubey, A. *et al.* A strategic review on processing routes towards highly efficient perovskite solar cells. *J. Mater. Chem. A* **6**, 2406–2431. https://doi.org/10.1039/c7ta08277k (2018).
3. Lee, J.-W. *et al.* Formamidinium and cesium hybridization for photo- and moisture-stable perovskite solar cell. *Adv. Energy Mater.* https://doi.org/10.1002/aenm.201501310 (2015).
4. Li, N. *et al.* Microscopic degradation in formamidinium-cesium lead iodide perovskite solar cells under operational stressors. *Joule* **4**, 1743–1758. https://doi.org/10.1016/j.joule.2020.06.005 (2020).
5. Peng, Z. *et al.* Cs0.15FA0.85PbI3/CsxFA1-xPbI3 core/shell heterostructure for highly stable and efficient perovskite solar cells. *Cell Rep. Phys. Sci.* https://doi.org/10.1016/j.xcrp.2020.100224 (2020).

6. Alwarappan, G. *et al.* Role of organic cation in modern lead-based perovskites. *Sol. Energy* **189**, 86–93. https://doi.org/10.1016/j.solener.2019.07.028 (2019).
7. Mehdizadeh, A., Akhtarianfar, S. F. & Shojaei, S. Role of methylammonium rotation in hybrid halide MAPbX3 (X = I, Br, and Cl) perovskites by a density functional theory approach: Optical and electronic properties. *J. Phys. Chem. C* **123**, 6725–6734. https://doi.org/10.1021/acs.jpcc.8b11422 (2019).
8. Gao, L.-K., Tang, Y.-L. & Diao, X.-F. Theoretical study on photoelectric properties of FAPbI3 doped with Ge. *Mater. Res. Express.* https://doi.org/10.1088/2053-1591/ab9edf (2020).
9. Xu, X. L. *et al.* Molecular ferroelectrics-driven high-performance perovskite solar cells. *Angew. Chem. Int. Ed. Engl.* **59**, 19974–19982. https://doi.org/10.1002/anie.202008494 (2020).
10. Ma, J. & Wang, L. W. Nanoscale charge localization induced by random orientations of organic molecules in hybrid perovskite CH3NH3PbI3. *Nano Lett.* **15**, 248–253. https://doi.org/10.1021/nl503494y (2015).
11. Bakulin, A. A. *et al.* Real-time observation of organic cation reorientation in methylammonium lead iodide perovskites. *J. Phys. Chem. Lett.* **6**, 3663–3669. https://doi.org/10.1021/acs.jpclett.5b01555 (2015).
12. Hoehn, R. D., Francisco, J. S., Kais, S. & Kachmar, A. Role of water on the rotational dynamics of the organic methylammonium cation: A first principles analysis. *Sci. Rep.* **9**, 668. https://doi.org/10.1038/s41598-018-36900-4 (2019).
13. Motta, C. *et al.* Revealing the role of organic cations in hybrid halide perovskite CH3NH3PbI3. *Nat. Commun.* **6**, 7026. https://doi.org/10.1038/ncomms8026 (2015).
14. Bechtel, J. S., Seshadri, R. & Van der Ven, A. Energy landscape of molecular motion in cubic methylammonium lead iodide from first-principles. *J. Phys. Chem. C* **120**, 12403–12410. https://doi.org/10.1021/acs.jpcc.6b03570 (2016).
15. Gallop, N. P. *et al.* Rotational cation dynamics in metal halide perovskites: Effect on phonons and material properties. *J. Phys. Chem. Lett.* **9**, 5987–5997. https://doi.org/10.1021/acs.jpclett.8b02227 (2018).
16. Farshad Akhtarianfar, S., Shojaei, S. & Khameneh Asl, S. Organic cation rotation in HC(NH2)2PbI3 perovskite solar cells: DFT and DOE approach. *Sol. Energy* **220**, 70–79. https://doi.org/10.1016/j.solener.2021.03.027 (2021).
17. Fabini, D. H. *et al.* Universal dynamics of molecular reorientation in hybrid lead iodide perovskites. *J. Am. Chem. Soc.* **139**, 16875–16884. https://doi.org/10.1021/jacs.7b09536 (2017).
18. Ou, Q. *et al.* Band structure engineering in metal halide perovskite nanostructures for optoelectronic applications. *Nano Mater. Sci.* **1**, 268–287. https://doi.org/10.1016/j.nanoms.2019.10.004 (2019).
19. Kresse, G. & Furthmüller, J. Efficient iterative schemes for ab initio total-energy calculations using a plane-wave basis set. *Phys. Rev. B* **54**, 11169–11186. https://doi.org/10.1103/PhysRevB.54.11169 (1996).
20. Kresse, G. & Furthmüller, J. Efficiency of ab-initio total energy calculations for metals and semiconductors using a plane-wave basis set. *Comput. Mater. Sci.* **6**, 15–50. https://doi.org/10.1016/0927-0256(96)00008-0 (1996).
21. Perdew, J. P., Burke, K. & Ernzerhof, M. Generalized gradient approximation made simple. *Phys. Rev. Lett.* **77**, 3865–3868. https://doi.org/10.1103/PhysRevLett.77.3865 (1996).
22. Thonhauser, T. *et al.* Van der Waals density functional: Self-consistent potential and the nature of the van der Waals bond. *Phys. Rev. B* **76**, 125112. https://doi.org/10.1103/PhysRevB.76.125112 (2007).
23. Monkhorst, H. J. & Pack, J. D. Special points for Brillouin-zone integrations. *Phys. Rev. B* **13**, 5188–5192. https://doi.org/10.1103/PhysRevB.13.5188 (1976).
24. Momma, K. & Izumi, F. VESTA 3for three-dimensional visualization of crystal, volumetric and morphology data. *J. Appl. Crystallogr.* **44**, 1272–1276. https://doi.org/10.1107/s0021889811038970 (2011).
25. Wang, V., Xu, N., Liu, J., Tang, G. & Geng, W. *VASPKIT: A User-friendly Interface Facilitating High-throughput Computing and Analysis Using VASP Code*. (2019).
26. Mosconi, E., Umari, P. & De Angelis, F. Electronic and optical properties of MAPbX3 perovskites (X = I, Br, Cl): A unified DFT and GW theoretical analysis. *Phys. Chem. Chem. Phys.* **18**, 27158–27164. https://doi.org/10.1039/C6CP03969C (2016).
27. Khandy, S. A., Islam, I., Gupta, D. C., Khenata, R. & Laref, A. Lattice dynamics, mechanical stability and electronic structure of Fe-based Heusler semiconductors. *Sci. Rep.* **9**, 1475. https://doi.org/10.1038/s41598-018-37740-y (2019).
28. Khandy, S. A. *et al.* Electronic structure, thermomechanical and phonon properties of inverse perovskite oxide (Na_3OCl): An ab initio study. *Int. J. Energy Res.* **44**, 2594–2603. https://doi.org/10.1002/er.4982 (2020).
29. Wang, S., Xiao, W.-B. & Wang, F. Structural, electronic, and optical properties of cubic formamidinium lead iodide perovskite: A first-principles investigation. *RSC Adv.* **10**, 32364–32369. https://doi.org/10.1039/d0ra06028c (2020).
30. Weller, M. T., Weber, O. J., Frost, J. M. & Walsh, A. Cubic perovskite structure of black formamidinium lead iodide, α-[HC(NH2)2]PbI3, at 298 K. *J. Phys. Chem. Lett.* **6**, 3209–3212. https://doi.org/10.1021/acs.jpclett.5b01432 (2015).
31. Oku, T. Crystal structures of perovskite halide compounds used for solar cells. *Rev. Adv. Mater. Sci.* **59**, 264–305. https://doi.org/10.1515/rams-2020-0015 (2020).
32. Amat, A. *et al.* Cation-induced band-gap tuning in organohalide perovskites: Interplay of spin-orbit coupling and octahedra tilting. *Nano Lett.* **14**, 3608–3616. https://doi.org/10.1021/nl5012992 (2014).
33. Ghosh, D., Walsh Atkins, P., Islam, M. S., Walker, A. B. & Eames, C. Good vibrations: Locking of octahedral tilting in mixed-cation iodide perovskites for solar cells. *ACS Energy Lett.* **2**, 2424–2429. https://doi.org/10.1021/acsenergylett.7b00729 (2017).
34. Yun, S., Zhou, X., Even, J. & Hagfeldt, A. Theoretical treatment of CH3 NH3 PbI3 perovskite solar cells. *Angew. Chem. Int. Ed. Engl.* **56**, 15806–15817. https://doi.org/10.1002/anie.201702660 (2017).
35. Li, Z. *et al.* Stabilizing perovskite structures by tuning tolerance factor: Formation of formamidinium and cesium lead iodide solid-state alloys. *Chem. Mater.* **28**, 284–292. https://doi.org/10.1021/acs.chemmater.5b04107 (2015).
36. Kawachi, S. *et al.* Structural and thermal properties in formamidinium and Cs-mixed lead halides. *J. Phys. Chem. Lett.* **10**, 6967–6972. https://doi.org/10.1021/acs.jpclett.9b02750 (2019).
37. Mattoni, A., Filippetti, A., Saba, M. I. & Delugas, P. Methylammonium rotational dynamics in lead halide perovskite by classical molecular dynamics: The role of temperature. *J. Phys. Chem. C* **119**, 17421–17428. https://doi.org/10.1021/acs.jpcc.5b04283 (2015).
38. Egger, D. A., Rappe, A. M. & Kronik, L. Hybrid organic-inorganic perovskites on the move. *Acc. Chem. Res.* **49**, 573–581. https://doi.org/10.1021/acs.accounts.5b00540 (2016).
39. Even, J., Pedesseau, L., Jancu, J.-M. & Katan, C. Importance of spin-orbit coupling in hybrid organic/inorganic perovskites for photovoltaic applications. *J. Phys. Chem. Lett.* **4**, 2999–3005. https://doi.org/10.1021/jz401532q (2013).
40. Prasanna, R. *et al.* Band gap tuning via lattice contraction and octahedral tilting in perovskite materials for photovoltaics. *J. Am. Chem. Soc.* **139**, 11117–11124. https://doi.org/10.1021/jacs.7b04981 (2017).
41. Gruninger, H. *et al.* Microscopic (dis)order and dynamics of cations in mixed FA/MA lead halide perovskites. *J. Phys. Chem. C Nanomater. Interfaces* **125**, 1742–1753. https://doi.org/10.1021/acs.jpcc.0c10042 (2021).
42. Taylor, V. C. A. *et al.* Investigating the role of the organic cation in formamidinium lead iodide perovskite using ultrafast spectroscopy. *J. Phys. Chem. Lett.* **9**, 895–901. https://doi.org/10.1021/acs.jpclett.7b03296 (2018).
43. Xiao, Z., Zhou, Y., Hosono, H., Kamiya, T. & Padture, N. P. Bandgap optimization of perovskite semiconductors for photovoltaic applications. *Chemistry* **24**, 2305–2316. https://doi.org/10.1002/chem.201705031 (2018).
44. Hu, Z. *et al.* A review on energy band-gap engineering for perovskite photovoltaics. *Solar RRL* **3**, 25. https://doi.org/10.1002/solr.201900304 (2019).
45. Zhou, Y., Chen, J., Bakr, O. M. & Sun, H.-T. Metal-doped lead halide perovskites: Synthesis, properties, and optoelectronic applications. *Chem. Mater.* **30**, 6589–6613. https://doi.org/10.1021/acs.chemmater.8b02989 (2018).

46. Jing, Y., Liu, Y., Zhao, J. & Xia, Z. Sb3+ doping-induced triplet self-trapped excitons emission in lead-free Cs2SnCl6 nanocrystals. *J. Phys. Chem. Lett.* **10**, 7439–7444. https://doi.org/10.1021/acs.jpclett.9b03035 (2019).

Acknowledgements
Financial support from the National Natural Science Foundation of China (Nos. 61904036, 62074044 and 61675049), Zhongshan-Fudan Joint Innovation Center and Jihua Laboratory Projects of Guangdong Province (X190111UZ190).

Author contributions
S.Y.L. conducted the project, performed the theoretical calculation and wrote the manuscript. All authors contributed to the discussion of content. S.Y.L. drew Figs. 1, 7, 8, S1, S2 and S3. J.W. drew Figs. 2, 3 and 4. Z.T.D drew Figs. 5 and 6. Z.H. and W.L.Z. revised the article structure and English expression of this manuscript. H.Z checked and corrected the manuscript. F.X.X. and R.Q.G. conceived the project and revised the manuscript.

Competing interests
The authors declare no competing interests.

Additional information
Supplementary Information The online version contains supplementary material available at https://doi.org/10.1038/s41598-021-99621-1.

Correspondence and requests for materials should be addressed to R.G. or F.X.

Reprints and permissions information is available at www.nature.com/reprints.

Publisher's note Springer Nature remains neutral with regard to jurisdictional claims in published maps and institutional affiliations.